Case Studies in Thermal Engineering 41 (2023) 102599

Contents lists available at ScienceDirect

Case Studies in Thermal Engineering

journal homepage: www.elsevier.com/locate/csite

Atomistic insights into the heat conductance across the interfaces between erythritol and different metals: A non-equilibrium molecular dynamics study

Biao Feng [a,b], Jia Liu [b], Yi Zeng [c,d,**], Li-Wu Fan [b,e,*]

[a] PowerChina HuaDong Engineering Corporation Limited, Hangzhou, Zhejiang, 311122, PR China
[b] Institute of Thermal Science and Power Systems, School of Energy Engineering, Zhejiang University, Hangzhou, Zhejiang, 310027, PR China
[c] Department of Mechanical Engineering, Auburn University, Auburn, AL, 36849, USA
[d] National Renewable Energy Laboratory, Golden, CO, 80401, USA
[e] State Key Laboratory of Clean Energy Utilization, Zhejiang University, Hangzhou, Zhejiang, 310027, PR China

ARTICLE INFO

Keywords:
Molecular dynamics
Polyol phase change material
Interfacial heat conductance
Interfacial contact ratio
Lattice vibrations

ABSTRACT

The heat conductance across the interface between a phase change material (PCM) and the metal shell is important for thermal design of latent heat storage systems. Non-equilibrium molecular dynamics simulations were carried out in this work to unravel, at the atomistic level, the interfacial heat conductance mechanisms between erythritol (the most promising medium-temperature polyol PCM) and two different metals (i.e., copper and aluminum). The interfacial contact ratio was introduced as a parameter to represent different contact conditions at the interfaces, for example, different surface roughness levels of the metals. It was found that with the increase of interfacial contact ratio, the temperature difference between the erythritol/metal interfaces decreases, whereas the interfacial heat transfer coefficient increases gradually. At the perfect contact condition, i.e., the interfacial contact ratio reaches 100%, the interfacial heat transfer coefficients across the erythritol/Cu and erythritol/Al interfaces were predicted to be 398 ± 26 MW/m^{2}K and 544 ± 11 MW/m^{2}K, respectively. The interfacial heat conductance of erythritol/Al is better than that of erythritol/Cu. The mismatch of atomic spectral density across the interfaces between erythritol and the two metals was analyzed and distinguished. These results could guide the selection of packaging materials and the thermal design of erythritol-based latent heat storage systems.

Nomenclature

A_{convex}	convex surface area (nm^2)
A_{metal}	cross-sectional area of metal (nm^2)
Al	aluminium
C	carbon
Cu	copper

* Corresponding author. Institute of Thermal Science and Power Systems, School of Energy Engineering, Zhejiang University, Hangzhou, Zhejiang, 310027, PR China.
** Corresponding author. Department of Mechanical Engineering, Auburn University, Auburn, AL, 36849, USA.
E-mail addresses: Yi.Zeng@nrel.gov (Y. Zeng), liwufan@zju.edu.cn (L.-W. Fan).

https://doi.org/10.1016/j.csite.2022.102599
Received 1 June 2022; Received in revised form 15 October 2022; Accepted 23 November 2022
Available online 25 November 2022

$\mathbf{F}_{jl}$	inter-molecular force of atom l on atom j (kJ/mol·nm)
G	interfacial heat transfer coefficient (MW/m^{2}K)
i	imaginary number
H	hydrogen
j	j-th atom or molecule
J_{int}	heat current through interface (kJ/mol·fs)
k_{B}	Boltzmann constant
l	l-th atom or molecule
m_l	mass of the l-th atom or molecule (g/mol)
N_{atom}	number of the atoms in a molecule
N_{mol}	number of the molecules
O	oxygen
R	atoms contained in erythritol
S	atoms of metal
t	time (fs)
T	temperature (K)
$\mathbf{v}_l$	velocity of the l-th atom (nm/fs)
$\mathbf{v}_j$	velocity of the j-th atom (nm/fs)
$\mathbf{V}_{j,l}$	velocity of atom l in the molecule j (nm/fs)
x,y,z	the Cartesian coordinate

Greek symbols

μ	interfacial contact ratio
ν	frequency (THz)
π	ratio of circumference to diameter
η	overlap factor of vibrational density of states

1. Introduction

Latent heat storage technology can alleviate the contradiction between demand and supply of thermal energy, ameliorate the conversion efficiency of thermal energy, and promote the comprehensive cascade utilization of solar energy and industrial waste heat. High-performance phase change materials (PCMs) act a pivotal part in the development of latent heat storage technology. In recent years, polyol PCMs, which exhibit high latent heat of fusion, have attracted much attention in the medium temperature range of about 370–520 K [1]. Erythritol is one of the representative polyol PCMs with very high storage density due to the multiple high-polarity hydroxyl groups in its molecular structure [2]. However, the thermal conductivity of erythritol is low, about 0.7 W/mK at 300 K [3]. This shortcoming limits the heat exchange ratio between erythritol and heat exchange medium, which greatly affects the heat storage/retrieval performance in the periodic phase transition cycle of the latent heat storage system. Therefore, it is essential to meliorate the thermal conductivity of erythritol.

At present, a great amount of investigations have tried various methods to raise the thermal conductivities of traditional PCMs. Some researchers have tried to combine PCMs with porous metal foam with high thermal conductivity, and prepared various PCM composites. Li et al. [4] impregnated erythritol into hydrophilic copper (Cu) foam with rough surfaces and obtained the Cu foam-templated composites. The thermal conductivities of such composites were 5 folds larger than that of pure erythritol. Meanwhile the heat retrieval rate of solar-thermal energy storage system based on such composites was as high as 85.8%.

However, there are few investigations on polyol PCM/metal foam composites. More researches were focused on the melting and thermophysical properties of other PCMs/metal foam composites through experiments [5] and simulations [6]. Jin et al. [5] investigated the influence of pore diameter on the melting rates and heat transfer ability of paraffin/Cu foam by adopting Cu foam with different porosities. They found that the melting rates of composites having the pore diameters of 30 and 50 ppi were almost identical, both of which were much faster than the melting rates of 15 ppi at the superheated wall temperature of 30 K. This result indicated that the reduction of pore size can meliorate the thermal conductivity of composites consisted of PCM/metal foam. However, their infrared thermograph shown the distinct temperature differences between the metal foam skeleton and paraffin in melting process, which means there were large thermal contact resistances (TCRs) between Cu foam and paraffin. Wang et al. [6] utilized the finite element method to decide the effective thermal conductivity and melting efficiency of PCM/metal foam composites. Their results implied that the effective thermal conductivity of the composites is inversely proportional to the actual porosity of metal foam. When being heated, the PCMs close to the heat source as well as the metal foam skeleton melt first, and then the PCMs in the center melt gradually.

Therefore, it is necessary to investigate the TCR between the PCM and metal foam. Sadeghi et al. [7] proposed a theoretical model based on PCM/metal foam and predicted the TCR at interfaces of PCM/metal. They developed a graphical code to trace the allocation of contact points, thereby estimating the actual area of contact at the interfaces and calculating the PCM/Al foam composites' effective thermal conductivity. Their results implied that contact pressure, porosity, pore density and surface characteristics of metal foam will affect the actual contact area of PCMs and metal foam, thus affecting the TCR at interfaces of PCM/metal foam. Yang et al. [8] utilized

Hot Disk thermal constant analyzer and computed tomography methods to analyze the effects of internal void of Cu foam and porosity on the thermal conductivity of paraffin/Cu foam composites. Zheng et al. [9] carried on molecular dynamics (MD) simulations and then predicted the interfacial TCR of paraffin/metal. In contrast to their experimental measurements, their MD results indicated a similar tendency.

These aforementioned studies implied the large TCR between the interfaces of the PCM/metal foam composites, which will affect their interfacial heat transfer significantly. Moreover, when being packaged in a heat storage tank, the TCR between PCMs and the thin-walled metal shells will also affect the heat exchange rates of the whole latent heat storage system [10]. Therefore, it is necessary for researchers to carry out measurements and microscale studies on the thermal contact resistance between polyol PCM and metal shells. Feng et al. [11] proposed a novel steady-state heat-flow method and measured the TCR at the interfaces of erythritol/nickel silver, erythritol/stainless steel and erythritol/1060Al. Their results revealed the influences of interfacial contact pressure and surface roughness on the TCR, and proved the excellent interfacial heat transfer between erythritol and 1060Al. However, the micro interfacial heat conductance mechanism of erythritol/metal is difficult to be explained by macroscopic experiments.

Therefore, the interfacial heat transfer at interfaces between erythritol and different metals (Cu and Al) was investigated in this dissertation by performing non-equilibrium MD (NEMD) simulations. The interfacial heat transfer coefficient was predicted, and various interfacial contact ratios of erythritol/Cu and erythritol/Al were analyzed and compared. Moreover, in order to clarify the underlying mechanism on the thermal response at the interfaces of erythritol/metal, the vibrational density of states, namely VDOS, was determined. The mismatches of phonon spectra of the interface of erythritol and different metals were analyzed and distinguished at the phonon level.

2. Methodology

2.1. Simulation details

To elucidate the heat conductance characteristics between erythritol and metal interfaces in the heat storage system, classical MD methods were employed to provide an atomistic mechanism of interfacial heat transfer. The MD simulations performed here were the follow-up investigation of experimental measurements of Feng et al. [11]. Because the content of Cu in nickel silver is up to 60% and the content of aluminum (Al) in 1060Al is as high as 99.6%, the metal models were simplified to single crystal Cu and single crystal Al. Fig. 1 plots the simulation systems of erythritol/Cu and erythritol/Al. The crystal structure of erythritol was constructed based on its unit cell (a = 12.81 Å, b = 12.81 Å, c = 6.81 Å, $\alpha = \beta = \gamma = 90°$) [12] with a size of 17 nm × 4 nm × 4 nm [9]. The crystal models of Cu and Al were made according to the lattice parameters of Cu (a = b = c = 3.614 Å, $\alpha = \beta = \gamma = 90°$) [13], and the lattice parameters of Al (a = b = c = 4.049 Å, $\alpha = \beta = \gamma = 90°$) [14], respectively. Similarly, the size of the simulation systems of Cu and Al were both set to 10 nm × 4 nm × 4 nm [9]. It must also be mentioned that the simulation investigation here aims to reveal the underlying mechanisms and characteristics of heat transfer across the interfaces between polyol PCMs and metal, not to accurately predict the interfacial heat transfer coefficient. In fact, the TCR between thin-walled metal and erythritol has been measured experimentally in the authors' previous study [15]. Therefore, the size effect of the simulation system on heat conduction was not considered, and the size of the simulation system was set based on the previous reference [9], which has been verified to weaken the truncation effects effectively. The initial nano-gap between the interfaces of erythritol and the metal was set to 3 Å.

In the previous study, it has been found that the effects of hardness, surface roughness and contact pressure on the TCR between the interfaces of erythritol and multiple metals (SS304, nickel silver, and 1060Al) can be attributed to the change of actual contact area [15]. Therefore, the interfacial contact ratio μ is defined to characterize the surface contact quantitatively and to represent different contact conditions at the interfaces, which is given as:

$$\mu = \frac{A_{\text{convex}}}{A_{\text{metal}}} \times 100\%, \tag{1}$$

where A_{convex} represents the convex surface area of the metal block, and A_{metal} represents the cross-sectional area of the metal system.

As vividly plotted in Fig. 1, a symmetrical convex rectangular structure having a length of 0.6 nm was constructed at both ends of the contact surface between metal (Cu and Al) and erythritol, where the interfacial contact ratio μ between erythritol and metal was set

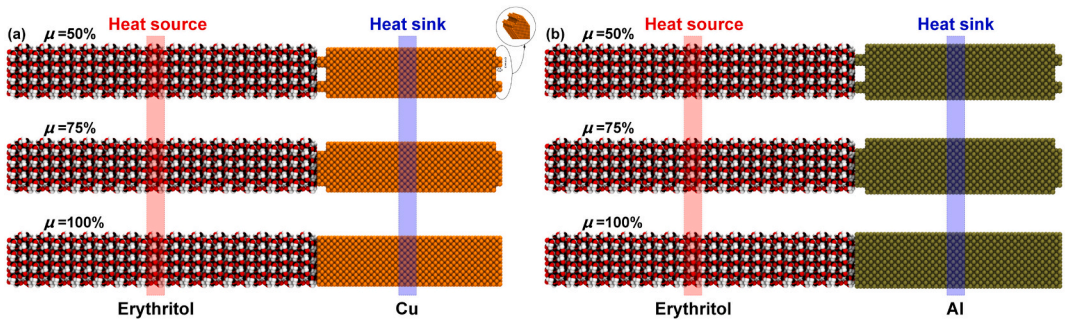

Fig. 1. NEMD simulation system of (a) erythritol/Cu and (b) erythritol/Al with different interfacial contact ratio.

to three different values (50%, 75% and 100%) and compared. It is essential to mention that the geometry and interfacial contact ratio in Fig. 1 are defined to represent different contact conditions, and reveal the underlying mechanisms and characteristics of interfacial heat transfer between polyol PCMs and metal. Considering that the investigation of this work is not for quantitative calculating the interfacial heat transfer, but for studying the variation rule at the interfaces. Therefore, even if the length of convex rectangular structure was tested with 0.4 nm, 0.6 nm and 0.8 nm, which showed similar results, only the results of the convex rectangular structure with a length of 0.6 nm were presented. Since the periodic boundary was adopted in all the three-dimensional directions (x, y and z), the convex structures were set on both sides of the metal system. Moreover, it is significant to highlight that the heat conduction between erythritol/metal interfaces was only investigated and analyzed in the phonon scale, and the electron transport and interfacial electron-transfer were not involved, which is beyond the scope of this work and needs further in-deep studies.

EAM force field was utilized to describe the molecular interaction of Cu and Al, which has been widely used to describe the interatomic interactions between metals [16] and the corresponding force field parameters were obtained from the literature [17,18]. In this work, the thermal conductivity of Cu an Al were predicted to be about 172 ± 17 W/mK and 361 ± 22 W/mK respectively, which were consistent with the literature [19]. Since the temperature gradient of the metals can be obtained during simulating the interfacial heat conduction between erythritol and metals by using NEMD methods, the thermal conductivity of metals can thus be calculated based on the Fourier's law of heat conduction. The specific calculation method will be described in detail in Section 2.2. The molecular motions of erythritol were characterized by GROMOS force field [20], which has been tested in erythritol specifically [3]. The intermolecular interaction between metal and erythritol was identified by the 12–6 Lennard Jones potential, which has been tested and utilized widely [21,22]. Table 1 listed the corresponding force field parameters, where the interactions of Cu and Al were obtained from reference [23]. In addition, the intermolecular interaction parameters between metal and erythritol were calculated by the Lorentz-Berthelot mixing rules [24].

2.2. NEMD methods

In this study, MD simulations were performed based on LAMMPS [25]. The Velocity Verlet algorithm [26] and periodic boundary were adopted to solve the equation of motion, and the Particle-Particle-Particle-Mesh (PPPM) algorithm [27] was utilized to calculate the Coulomb interaction in the long-range with a calculation precision of 10^{-6}. The time step of the numerical integration was 0.5 fs. The NEMD method [28] and enhanced heat exchange (eHEX) algorithm [29] were employed to analyze the thermodynamics properties and calculate the interfacial heat transfer coefficient at interfaces between erythritol and metal with different interfacial contact ratios μ. The isobaric-isothermic ensemble (NPT) was adopted with isotropic pressure coupling so as to maintain the simulation system at 300 K and 0.1 MPa for 2 ns As shown in Fig. 1, each simulation system of erythritol/metal was then divided into 15 slides equally along the heat flow (x direction). One slide in the middle of erythritol served as the heat source, and one slide in the middle of metal served as the heat sink. The eHEX algorithm exchanged the kinetic energy of the heat sink with the heat source under the micro-canonical (NVE) ensemble, so as to form a constant heat current. Under the periodic boundary condition, such settings can ensure the heat current flows across all interfaces. In the simulation systems of this work, all of the imposed total heat currents were 0.005 kcal/mol·fs (0.02092 kJ/mol·fs, namely 0.21682 eV/ps). The simulation time under the NVE condition with eHEX algorithm was set as 5 ns, so as to reach thermodynamic equilibrium. The temperature data of the simulation system was then computed and averaged within 3 ns Due to the small number of atoms in the interface layer, the temperature usually fluctuates greatly, resulting in a large temperature difference. In order to eliminate the calculation error of the temperature at interfacial regions, the linear fitting temperature at the interface was determined by using the least square method. The density catastrophe point of the simulation system of erythritol/metal was calculated, which was regarded as the interface. In order to determine the temperature difference ΔT at interfaces of erythritol/metal, the temperature distributions of erythritol and metal were then plotted and extended to the interface, respectively. Hence, the interfacial heat transfer coefficient was determined by:

$$G = \frac{J_{\text{int}}}{\Delta T}. \tag{2}$$

where J_{int} represents the heat current across the erythritol/metal interfaces in the NEMD simulation, which can be decomposed into the intermolecular vdW interaction term J_{vdW} and Coulombic interaction term J_{Cl} and identified by [30]:

$$J_{\text{int}} = \frac{1}{2}\sum_{j\in S}\sum_{l\in R}\left[\mathbf{F}_{jl}\cdot\left(\mathbf{v}_j + \mathbf{v}_l\right)\right], \tag{3}$$

Table 1
The atomic type and non-bonded interaction parameters of erythritol and metals.

atom	m (g/mol)	q (e)	ε (kJ/mol)	σ (Å)
tail C	12.0110	0.129–0.160	0.277406	3.581179284
body C	12.0110	0.227–0.255	0.277406	3.581179284
tail H	1.0080	0.06–0.07	0.118381	2.373408143
body H	1.0080	0.018–0.028	0.118381	2.373408143
hydroxyl O	15.9994	−0.679 ~ −0.715	0.849607	2.954841833
hydroxyl H	1.0080	0.452–0.453	0.000000	0.0000000
Al	26.9810	0	48.94673	2.5736600
Cu	63.5400	0	50.20992	2.2972600

where $\mathbf{F}_{jl}$ is the force exerted from j-th atom to l-th atom, including the Coulombic and vdW force. S and R are two neighboring molecular layers, where S represents erythritol and R means metal. The $\mathbf{v}_j$ is the j-th atom's velocity in erythritol and $\mathbf{v}_l$ is the l-th atom's velocity in metal, respectively. In the simulation run, the velocities of atoms located within the potential cutoff distance from the interfaces are sampled at intervals of 5 ns for the duration of the simulation. This method has been adopted in CNT, alkanes and sugar alcohols [30,31]. It should be noted that the heat current calculated here is used to verify the input heat flow, so as to ensure the accuracy of the simulations.

2.3. Data reduction

So as to supply a microscale investigation of the thermal response, the phonon-level VDOS of the material was determined by performing the Fourier transform on the velocity autocorrelation function. Hence, VDOS was identified as a function of vibration frequency ν as follows [32]:

$$\mathrm{VDOS}(\nu)=\frac{2}{k_B T N_{\mathrm{mol}} N_{\mathrm{atom}}}\sum_{n=x,y,z}\sum_{j=1}^{N_{\mathrm{mol}}}\sum_{l=1}^{N_{\mathrm{atom}}}\lim_{t\to\infty}\frac{m_l}{2t}\left|\int_{-t}^{t}\mathbf{v}_{j,l}(t)e^{-i2\pi\nu t}\mathrm{d}t\right|^2, \tag{4}$$

where N_{mol} means the number of molecules, N_{atom} means the atom number in a molecule, $\mathbf{v}_{j,l}$ represents the velocity of the l-th atom relative to the j-th molecule, m_l means the l-th atom's molar mass, k_{B} represents Boltzmann constant, t represents time, x, y and z mean the Cartesian coordinate. It should be mentioned that the VDOS was calculated at the interfaces of erythritol/Cu and erythritol/Al with a cutoff radius of 1.4 nm [31].

Moreover, in order to decide the match of vibrational mode between the two materials and clarify the spectral heat flux, the VDOS overlap factor, namely η, was further identified [33]:

$$\eta=\frac{\int_0^{+\infty}\min[\mathrm{VDOS}_1(\nu),\mathrm{VDOS}_2(\nu)]\mathrm{d}\nu}{\int_0^{+\infty}\mathrm{VDOS}_1(\nu)\mathrm{d}\nu}, \tag{5}$$

where VDOS_1 and VDOS_2 represent the VDOS of two different types of materials, $\min[\mathrm{VDOS}_1(\nu), \mathrm{VDOS}_2(\nu)]$ means the smaller one between VDOS_1 and VDOS_2, namely the overlap of VDOS_1 and VDOS_2.

Therefore, the numerator in the overlap factor η represents the overlapping area of the VDOS of two materials, and the denominator of the overlap factor η represents the VDOS of one of the reference materials. A large value of overlap factor η indicates a high match of vibrational mode between the two materials.

3. Results and discussion

3.1. Interfacial heat conductance

According to the aforementioned NEMD method, the average temperature distribution of erythritol/metal can be obtained after applying the heating current to the simulation system. Fig. 2 presents the temperature gradient of erythritol/Cu systems with different interfacial contact ratios μ. Generally, the temperature distribution of erythritol/Cu is smooth. The temperature in the middle of erythritol system is the highest because of the existence of heat source, while the temperature in the middle of Cu is the lowest owing to the heat sink. Although the temperature decreases linearly along the heat flow, it can be obviously found that the temperature difference of the whole simulation system is mainly concentrated at the interface between erythritol and Cu. As shown in Fig. 2a, the interfacial temperature difference between erythritol and Cu is as high as 14.8 ± 0.5 K when the interfacial contact ratio μ is 50%. In contrast, when the interface contact ratio μ increases to 75% and 100%, the interfacial temperature differences between erythritol and

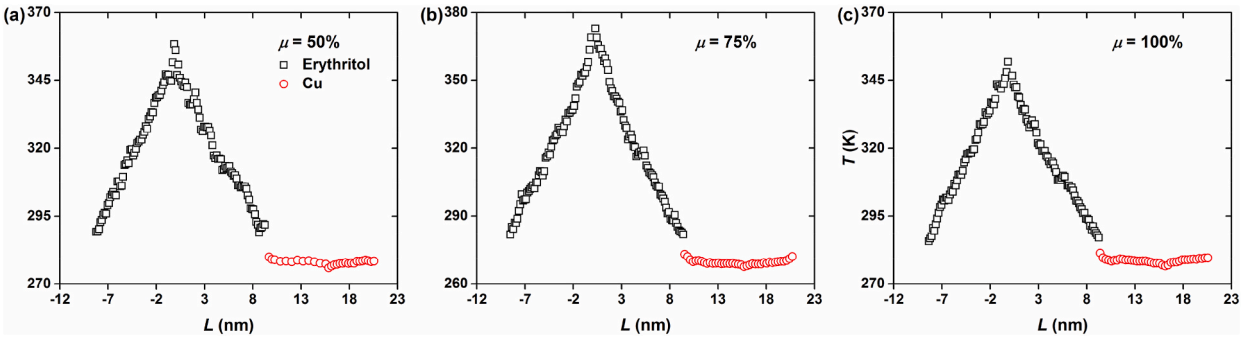

Fig. 2. Temperature gradient in the erythritol/Cu system under the NEMD method.

Cu are about 13.1 ± 0.5 K and 11.9 ± 0.4 K, respectively (seen in Fig. 2b and c). These results suggested that the interfacial temperature difference of erythritol/Cu decreases gradually with the increase of interfacial contact ratio μ.

Moreover, the temperature distributions of erythritol/Al systems are plotted in Fig. 3, which shows the similar tendency. The highest and lowest temperatures are observed in the middle of erythritol and Al, respectively. Due to the thermal conductivity of Al is obviously larger than that of erythritol, the slope of temperature gradient in erythritol is much higher than that of Al. Similarly, it is obvious to find that the temperature difference of the whole simulation system is mainly concentrated at the interfaces between erythritol and Al. As plotted in Fig. 3a, the interfacial temperature difference between erythritol and Al is as high as 9.9 ± 0.5 K with the interfacial contact ratio μ of 50%. By comparison, when the interface contact ratio μ increases to 75% and 100%, the interfacial temperature differences of erythritol/Al are 8.0 ± 0.4 K and 6.9 ± 0.4 K, respectively. Combined with Figs. 2 and 3, it can be concluded that no matter what the metal is, the temperature difference between erythritol and metal always decreases as increasing the interfacial contact ratio μ.

However, it should be noted that there are great differences in the temperature gradient between erythritol/Cu and erythritol/Al systems. When the cross-sectional area of erythritol, the cross-sectional area of metal and the interfacial contact ratio μ are consistent, the interfacial temperature difference of erythritol/Al is always ~5 K lower than that of erythritol/Cu. These results indicated that as compared to erythritol/Cu, erythritol/Al shows better interfacial heat transfer.

So as to quantify the interfacial heat transfer coefficient at erythritol/metal interfaces, the heat current across the interfaces of erythritol/metal was calculated according to Eq. (3) and presented in Fig. 4. The red dash line in Fig. 4 represents the time-averaged heat current through the interface at 300 K. As can be seen from Fig. 4a−4c, when the interfacial contact ratios μ are 50%, 75% and 100%, the heat current J_{int} across the erythritol/Cu interfaces are about 0.01939, 0.02143 and 0.02229 kJ/mol·fs respectively, which are basically in accord with the imposed heat current (0.02092 kJ/mol·fs). Meanwhile, similar results were found in the erythritol/Al simulation system. When interfacial contact ratio μ varies between 50% and 100%, the heat current J_{int} across the erythritol/Al interfaces varies from 0.01986 to 0.02125 kJ/mol·fs, coinciding with the imposed heat current. It should be pointed out that there are negative heat currents in Fig. 4, which implies the opposite heat current due to the corresponding interatomic forces [34].

When obtaining the value of heat current, the interfacial heat transfer coefficient G at erythritol/metal interfaces in solid phase was further determined based on Eq. (2) and presented in Fig. 5a. In general, the interfacial heat transfer coefficient G between interfaces of erythritol and metal increases as increasing the interfacial contact ratio μ, which is supported by the reduction of the interfacial temperature difference in Figs. 2 and 3. MD simulations shown that when the interfacial contact ratios μ are 50%, 75% and 100%, the interfacial heat transfer coefficients of erythritol/Cu are about 321 ± 21, 362 ± 12 and 398 ± 26 MW/m^{2}K, respectively. For the MD simulations of erythritol/Al, when the interfacial contact ratios μ are 50%, 75% and 100%, the interfacial heat transfer coefficients of erythritol/Al are about 383 ± 18, 471 ± 28 and 544 ± 11 MW/m^{2}K, respectively. It can be clearly found that under the same interfacial contact ratio μ, the interfacial heat transfer coefficients G at the interfaces of erythritol/Al are larger than that of erythritol/Cu, which are also consistent with the smaller temperature difference between erythritol and Al plotted in Fig. 3. Furthermore, it is worth noting that when the interfacial contact ratio μ increases from 50% to 100%, the increase of interfacial heat transfer coefficient G of erythritol/Cu is only 23.9%. However, for the erythritol/Al simulation system, when the interfacial contact ratio μ rises from 50% to 100%, the increase of interfacial heat transfer coefficient reaches up to 56.6%. These results demonstrated that the heat conductance of erythritol/Al is better than that of erythritol/Cu.

In addition, the above-mentioned heat transfer coefficient G obtained by MD simulations can be converted into the corresponding thermal contact resistance (TCR) by unit conversation. For erythritol/Cu, when the interfacial contact ratio μ are 50%, 75% and 100%, the TCR of erythritol and Cu are ~3.11×10^{-9}, ~2.76×10^{-9} and ~2.51×10^{-9} m^{2}K/W, respectively. For erythritol/Al, when the interfacial contact ratio μ are 50%, 75% and 100%, the TCR of erythritol and Al are ~2.61×10^{-9}, ~2.12×10^{-9} and ~1.84×10^{-9} m^{2}K/W, respectively. These results indicated that the interfacial TCR of erythritol/Al is smaller than that of erythritol/Cu, coinciding with the measured values acquired by Feng et al. [11]. Although the tendency of predicted TCR at erythritol/metal interfaces is consistent with the measurements, the TCR results calculated by MD simulation are far less than the measured results, namely, the heat transfer coefficients G obtained by MD simulations are far larger than the measured ones. This may be explained by the ideal interface topology constructed in MD simulations, where the micro-gap between interfaces of erythritol and metal is only 3 Å. However, this ideal structure hardly exists in reality. Under experimental conditions, the defects of the material are always much larger, which will

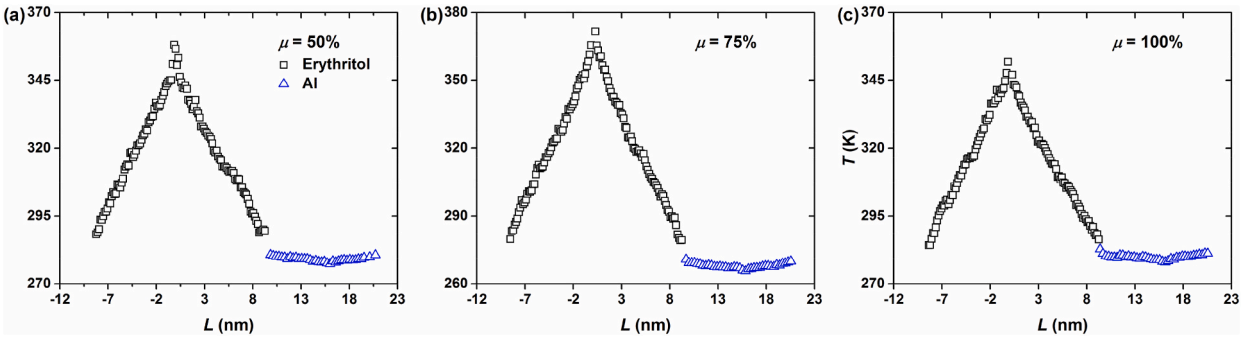

Fig. 3. Temperature gradient in the erythritol/Al system under the NEMD method.

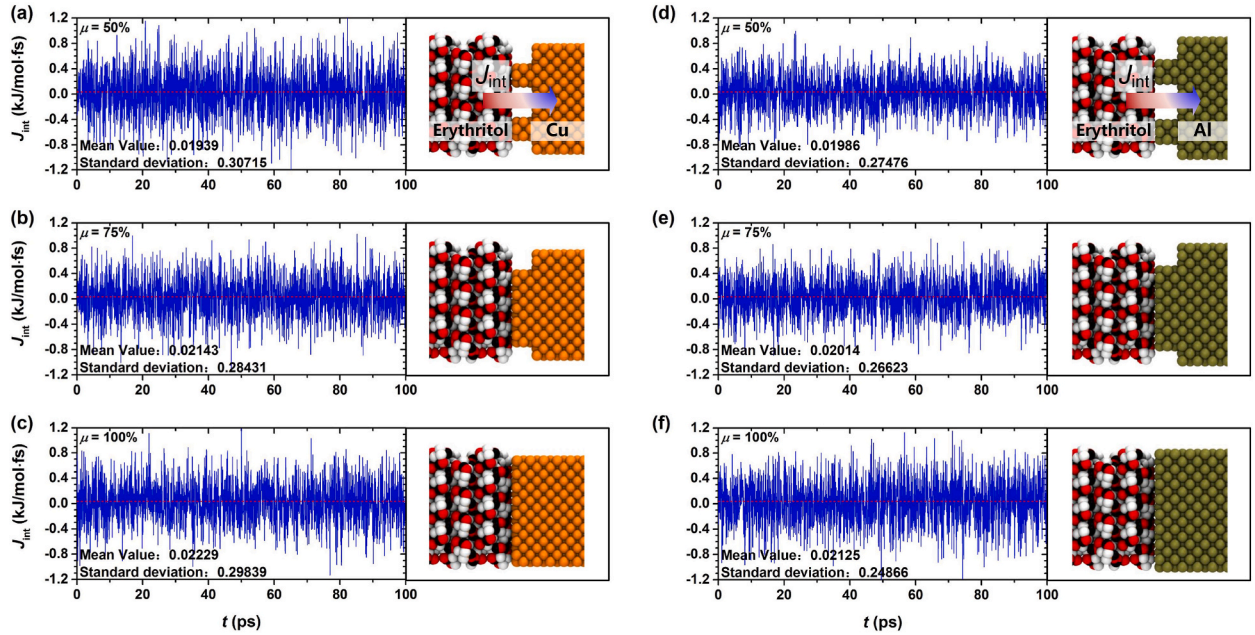

Fig. 4. The heat current across the erythritol/Cu interface with the interfacial contact ratio of (a) $\mu = 50\%$, (b) $\mu = 75\%$, (c) $\mu = 100\%$, and erythritol/Al interface with different interfacial contact ratio of (d) $\mu = 50\%$, (e) $\mu = 75\%$, (f) $\mu = 100\%$.

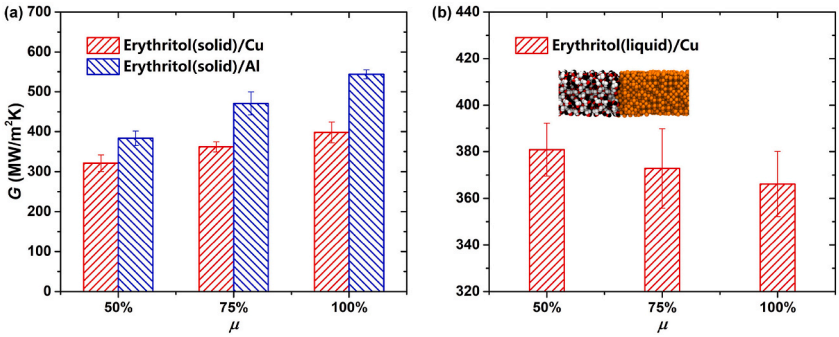

Fig. 5. The predicted interfacial heat transfer coefficient at the (a) erythritol/Cu and erythritol/Al interfaces in solid phase, and (b) erythritol(liquid)/Cu interfaces with different interfacial contact ratio.

greatly improve the interface phonon scattering and weaken the interfacial heat transfer [9]. Moreover, in the actual measurements, the gaps at the interfaces between erythritol and metal will also increase the interfacial TCR greatly [35].

In contrast to the solid erythritol, the interfacial heat transfer coefficient between liquid erythritol and Cu was also simulated, which basically showed opposite results. As plotted in Fig. 5b, liquid erythritol and Cu can fit well and keep close contact in the simulation run, resulting in higher interfacial heat transfer coefficients (381 ± 11 MW/m^{2}K) under lower interfacial contact ratios μ. One possible explanation for this result is that there is more contact area between liquid erythritol and metal under lower interfacial contact ratios μ. Moreover, it has been found that the interfacial convective heat-transfer coefficient can be significantly enhanced by increasing the liquid-solid interaction strength, roughness height and fractal dimension (topographical irregularity) [36,37]. When compared with smooth surface under flow conditions, the surface geometry could maintain liquid atoms contacting with the solid surface, contributing to large thermal conductance at a liquid-solid interface. However, in this work, there is no relative flow between liquid erythritol and solid metal interfaces. The actual contact area is the main factor affecting the interfacial heat conductance [7,11]. The erythritol and metals always keep close contact in the simulation run. Therefore, the effect of surface geometry on the solid-liquid interfacial heat conductance is not obvious. Since the study of this work focused on revealing the underlying mechanisms and characteristics of heat transfer across the interfaces between solid poly PCMs and metal, so as to explain the results of previous experiments [15], there are no more in-depth investigations on the interfacial heat transfer between liquid erythritol and metal.

3.2. *Vibrational density of state*

In order to reveal the underlying mechanism of interfacial heat conductance between erythritol and metal, and clarify the

difference between erythritol/Cu and erythritol/Al, the interfacial interaction energy between erythritol and metal was calculated. However, there are only van der Waals interactions between erythritol and different metals (Cu and Al). Based on the force field parameters in Table 1, the differences in the intermolecular interaction energy between erythritol and metals were limited. Therefore, the thermal response mechanism of interfacial heat conductance was analyzed in this dissertation. The variations of VDOS at the interfaces of erythritol/Cu and erythritol/Al were determined according to Eq. (4) with a cutoff radius of 1.4 nm [31].

Fig. 6 shows the atomic spectral density of carbon (C), oxygen (O), hydrogen (H) and Cu atoms in the erythritol/Cu simulation system with an interfacial contact ratio μ of 50%. As can be seen in Fig. 6, the VDOS of erythritol basically coincides between the y and z directions. The vibrational peaks of O atoms in erythritol are concentrated in the low-frequency region ($\nu < 20$ THz). While the maximum value of the vibrational peak of carbon atom is between 25 and 50 THz. Due to the number of hydrogen atoms in erythritol is the largest, the vibrational peaks of hydrogen atoms are the most obvious, and the extremum is concentrated in the high-frequency region (70–110 THz). However, in the x direction, the oxygen atoms show higher vibrational peaks than those of the y and z direction in the low-frequency region ($\nu < 20$ THz). These results suggested that the existence of interfaces has a strong effect on the lattice vibration. Along the heat current (x direction), more low-frequency phonons can be excited to participate in heat conduction, leading to more heat paths. When the frequency exceeds 120 THz, the calculated VDOS of erythritol is basically flat, and there is no peak in the high-frequency region. Moreover, the VDOS of Cu shows a consistent tendency in y and z directions. As plotted in Fig. 6, the vibrational peak of Cu appears in the low frequency region near 5 THz, where the peak value is about 1.95. However, in the x direction, the vibrational peak of Cu is wider than those of the y and z direction at the low frequency of 5 THz, which indicated that the vibrational energy of Cu is larger. Therefore, more low-frequency phonons are excited to participate in the heat conduction along the x direction.

Fig. 7 plots the atomic spectral density of C, O, H and Al atoms in the erythritol/Al simulation system with an interfacial contact ratio μ of 50%. Similarly, it can be observed that the VDOS of erythritol does not change much in y and z directions. The vibrational peaks of oxygen atoms in erythritol are concentrated in the low frequency region ($\nu < 20$ THz). Meanwhile, the extremum of the vibrational peak of carbon atoms is between 25 and 50 THz, and the extremum of the vibrational peak of hydrogen atoms is between 70 and 110 THz. Nevertheless, along the direction of heat current (x direction), the higher vibrational peak of oxygen is observed in the low frequency region ($\nu < 20$ THz). This result confirmed that more low-frequency phonons are excited in the direction of heat current, thus generating more heat paths.

Moreover, as shown in Fig. 7, the VDOS of Al is almost unchanged in y and z directions. The vibrational peak appears in the low frequency region (0–10 THz), where the peak value is about 2.41. In the x direction, the vibrational peak of Al atom at low frequency is also wider than those of y and z direction. These results suggested that as compared to the y and z direction, vibrational energy of Al in the x direction is higher and more low-frequency phonons are excited. Another interesting finding is that the vibrational peak of Al is higher than that of Cu, which will be explained in details in the follow-up analysis.

So as to better distinguish the differences between Cu and Al, the atomic spectral density of Cu and Al atoms in the erythritol/metal simulation systems with different interfacial contact ratios are presented in Figs. 8 and 9, respectively. As plotted in Fig. 8, the VDOS of Cu increases slightly when the interfacial contact ratio μ increases from 50% to 100%. However, the VDOS of Al increases obviously in Fig. 9, when the interfacial contact ratio rises from 50% to 100%. These results reflected that with the increase of interfacial contact ratio μ, more and more low-frequency phonons are excited. Moreover, it should be mentioned that these VDOS results are consistent with the variation of interfacial heat transfer coefficient between erythritol and metal. When the interfacial contact ratio increases, the variation of VDOS of Cu around the interfaces of erythritol/Cu is small. Therefore, the variation of interfacial heat transfer coefficient of erythritol/Cu with the interfacial contact ratio μ is finite. Nevertheless, the variation of VDOS of Al with the interfacial contact ratio μ is larger, reuslting in higher interfacial heat transfer coefficient at the interfaces of erythritol/Al.

One critical factor to identify the interfacial heat conductance is the overlap of the VDOS [38]. So as to quantify the differences of interfacial heat conductance between erythritol/Cu and erythritol/Al, the VDOS overlap factors η of erythritol/metal with the interfacial contact ratio μ were calculated based on Eq. (5), which are shown in Fig. 10. In general, the overlap factor η of VDOS is directly proportional to the interfacial contact ratio μ. When the interfacial contact ratio μ increases from 50% to 100%, the VDOS overlap factor η of erythritol/Cu increases from 0.276 to 0.283. In contrast, when the interfacial contact ratio μ of erythritol/Al rises from 50% to 100%, the VDOS overlap factor η increases from 0.324 to 0.346. These results indicated that with the increase of the interfacial contact ratio μ, the mismatch of VDOS at the erythritol/metal interfaces decreases, which promotes the interfacial heat

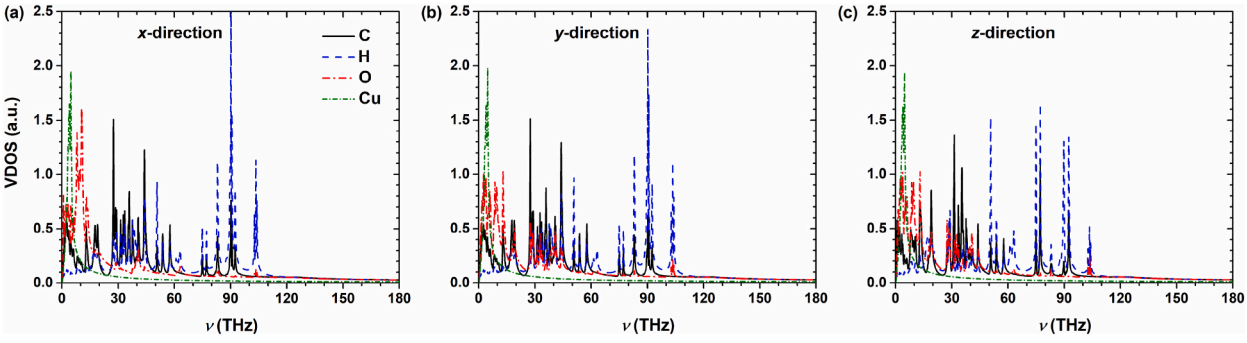

Fig. 6. The VDOS results of the erythritol/Cu system from lattice vibrations in the x, y, z directions.

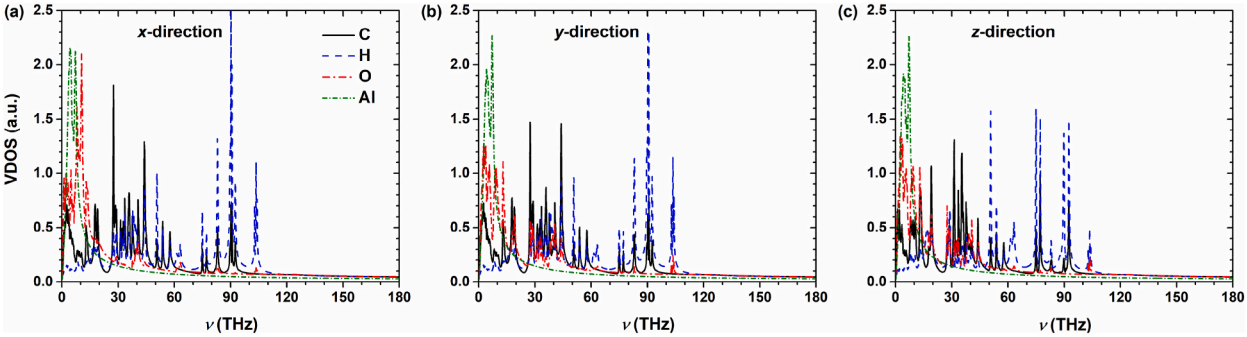

Fig. 7. The VDOS results of the erythritol/Al system from lattice vibrations in the *x*, *y*, *z* directions.

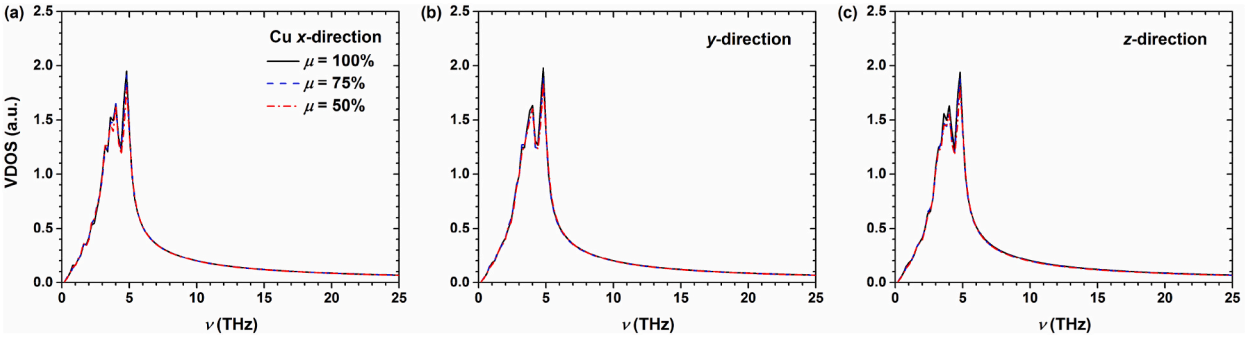

Fig. 8. Comparison of VDOS of Cu under different interfacial contact ratio in the *x*, *y*, *z* directions.

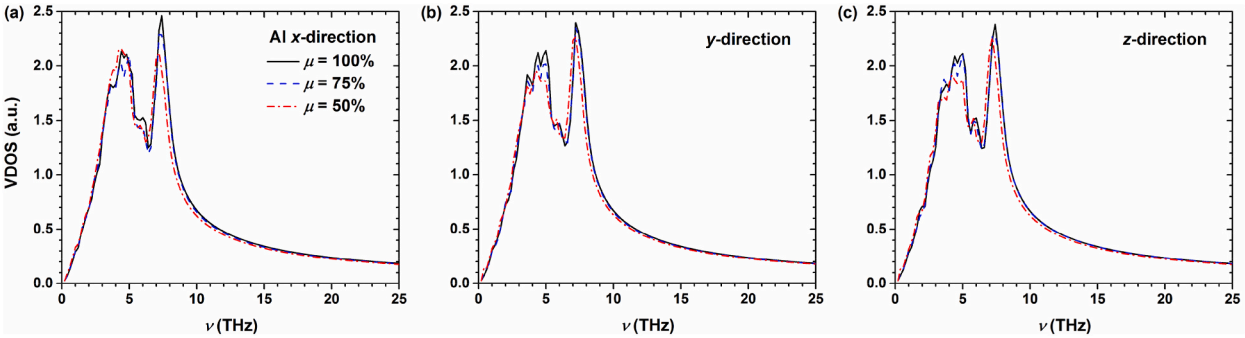

Fig. 9. Comparison of VDOS of Al under different interfacial contact ratio in the *x*, *y*, *z* directions.

conductance and increases the corresponding interfacial heat transfer coefficient *G*. Furthermore, with increasing the interfacial contact ratio μ, the variation of VDOS overlap factor of erythritol/Al is higher than that of erythritol/Cu, which accounts for the higher change rate of interfacial heat transfer coefficient at the interface between erythritol and Al. These findings revealed the connection between the interfacial heat transfer coefficient of erythritol/metal and interfacial contact ratio μ.

Moreover, it is noteworthy that the vibrational peak of Al is higher than that of Cu. Therefore, as shown in the blue bar chart of Fig. 10, the VDOS overlap factor η of erythritol/Al is also larger than that of erythritol/Cu. Therefore, the mismatch of phonon mode between erythritol and Al is low, and the corresponding interfacial heat conductance is excellent. In conclusion, the results of VDOS overlap factor η quantified the mismatch of the phonon modes of erythritol and metal at the interfaces, and elucidated the mechanism of the interfacial contact ratio μ on the interfacial heat conductance of the erythritol/metal simulation system. The lower mismatch of phonon modes of erythritol/Al will contribute to the larger interfacial heat transfer coefficient at interfaces between erythritol and Al.

4. Conclusions

In this study, NEMD simulations were carried out to elucidate the microscopic interfacial heat conductance characteristics of erythritol/Cu and erythritol/Al. The interfacial heat current with various interfacial contact ratios μ was defined, and the interfacial

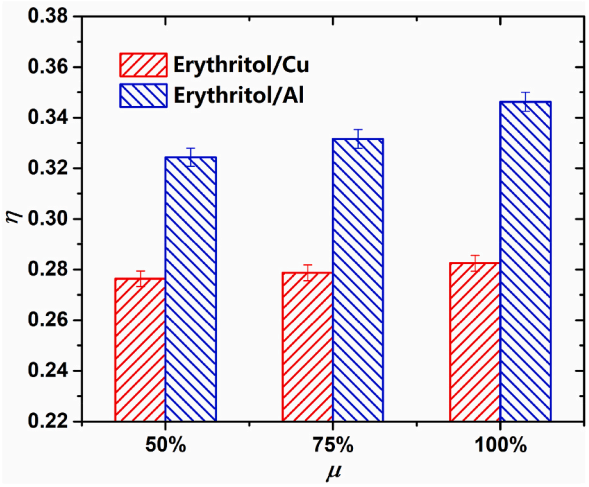

Fig. 10. Comparison of overlapping factors of VDOS at the interfaces between erythritol/Cu and erythritol/Al system with different interfacial contact ratio.

heat transfer coefficients were calculated quantitatively. The results suggested that no matter what the metal is, the temperature difference between erythritol and metal always decreases as increasing the interfacial contact ratio. The interfacial heat transfer coefficient increases gradually as increasing interfacial contact ratio. When the interfacial contact ratio rises from 50% to 100%, the increase of interfacial heat transfer coefficient at the interfaces between erythritol and Al reaches up to 56.6%. Moreover, the interfacial heat transfer coefficients of erythritol/Al are always larger than that of erythritol/Cu. When the interfacial contact ratio is 100%, the interfacial heat transfer coefficients of erythritol/Cu and erythritol/Al are 398 ± 26 MW/m^{2}K and 544 ± 11 MW/m^{2}K, respectively, indicating that interfacial heat conductance between erythritol and Al is better.

In order to reveal the undelying mechanism of interfacial heat conductance between erythritol and metal, the phonon-level analysis of VDOS was made. The results shown that along the direction of heat current, the higher vibrational peaks of O, Cu and Al atoms were observed in the lower frequency region. This result confirmed that more low-frequency phonons are excited in the direction of heat current, thus generating more heat paths. In contrast to Cu, the vibrational peak of Al is wider and higher, resulting in larger VDOS overlap factor between the interfaces of erythritol/Al. The large value of overlap factor indicated a low mismatch of phonon vibration between the erythritol and Al, which accounts for higher interfacial heat transfer coefficient at the interfaces between erythritol and Al. Furhtermore, when the interfacial contact ratio of erythritol/Al rises from 50% to 100%, the VDOS overlap factor increases from 0.324 to 0.346, which contribute to the increase of the interfacial heat conductance at the interfaces of erythritol/Al. These results acquired in this work are useful for the selection of packaging materials and the thermal design of latent heat storage systems.

Author statement

Biao Feng: Conceptualization, Investigation, Writing - Original Draft.
Jia Liu: Investigation, Writing - Original Draft.
Yi Zeng: Conceptualization, Writing - Review & Editing.
Li-Wu Fan: Supervision, Writing - Review & Editing, Funding acquisition.

Declaration of competing interest

The authors declare that they have no known competing financial interests or personal relationships that could have appeared to influence the work reported in this paper.

Data availability

Data will be made available on request.

Acknowledgments

This material is based upon work supported by the National Natural Science Foundation of China under Grant No. 52276088, and the China Postdoctoral Science Foundation under Grant No. 2022M722957. L.-W. Fan would like to thank a start-up fund granted by the “100 Talents Program” of Zhejiang University, and B. Feng would like to thank a fund granted by the “Strive for Excellent Doctoral Dissertation” of Zhejiang University.

References

[1] X.F. Shao, C. Wang, Y.J. Yang, B. Feng, Z.Q. Zhu, W.J. Wang, Y. Zeng, L.W. Fan, Screening of sugar alcohols and their binary eutectic mixtures as phase change materials for low-to-medium temperature latent heat storage. (I): non-isothermal melting and crystallization behaviors, Energy 160 (2018) 1078–1090.
[2] R. Anish, V. Mariappan, M.M. Joybari, et al., Performance comparison of the thermal behavior of xylitol and erythritol in a double spiral coil latent heat storage system, Therm. Sci. Eng. Prog. 15 (2020), 100441.
[3] B. Feng, L.W. Fan, Y. Zeng, et al., Atomistic insights into the effects of hydrogen bonds on the melting process and heat conduction of erythritol as a promising latent heat storage material, Int. J. Therm. Sci. 146 (2019), 106103.
[4] X. Li, J. Zhang, B. Fu, et al., Erythritol impregnated within surface-roughened hydrophilic metal foam for medium-temperature solar-thermal energy harvesting, Energy Convers. Manag. 222 (2020), 113241.
[5] H.Q. Jin, L.W. Fan, M.J. Liu, et al., A pore-scale visualized study of melting heat transfer of a paraffin wax saturated in a copper foam: effects of the pore size, Int. J. Heat Mass Tran. 112 (2017) 39–44.
[6] G. Wang, G. Wei, C. Xu, et al., Numerical simulation of effective thermal conductivity and pore-scale melting process of PCMs in foam metals, Appl. Therm. Eng. 147 (2019) 464–472.
[7] E. Sadeghi, S. Hsieh, M. Bahrami, Thermal conductivity and contact resistance of metal foams, J. Phys. Appl. Phys. 44 (12) (2011), 125406.
[8] X. Yang, X. Zheng, Z. Yang, et al., Effects of morphology and internal voids of copper ribs on heat transfer performance in copper foam/paraffin composite phase change materials, Int. J. Heat Mass Tran. 152 (2020), 119526.
[9] X. Zheng, X. Wang, T. Zhang, et al., Study on the interfacial thermal conductance between metals and phase change materials, Int. J. Heat Mass Tran. 168 (48) (2021), 120823.
[10] M.K. Rathod, J. Banerjee, Thermal performance enhancement of shell and tube latent heat storage unit using longitudinal fins, Appl. Therm. Eng. 75 (2015) 1084–1092.
[11] B. Feng, Y.H. Zhang, J. Tu, et al., Correlating the thermal contact resistance between metal/erythritol interfaces with surface roughness and contact pressure, Int. J. Heat Mass Tran. 176 (2021), 121407.
[12] A. Shimada, Crystal structure and lattice energy of i-erythritol. i. crystal structure of i-erythritol, Bull. Chem. Soc. Jpn. 22 (1959) 325–329.
[13] M.E. Straumanis, L.S. Yu, Lattice parameters, densities, expansion coefficients and perfection of structure of Cu and of Cu–In α phase, Acta Crystallogr. 25 (6) (2014) 676–682.
[14] S.H. Kellington, D. Loveridge, J.M. Titman, The lattice parameters of some alloys of lithium, J. Phys. Appl. Phys. 2 (8) (1969) 1162–1163.
[15] B. Feng, Y.H. Zhang, J. Tu, et al., Determination on the thermal conductivity and thermal contact resistance of thin composite phase change films as a thermal interfacial material, Case Stud. Therm. Eng. 33 (2022), 101979.
[16] Z. Xu, D. Ge, L. Zhang, Simulation and prediction on phonon thermal conductivity of Al/Cu interface, J. Phys. Chem. Solid. 122 (2018) 184–188.
[17] K.W. Jacobsen, J.K. Norskov, M.J. Puska, Interatomic interactions in the effective-medium theory, Phys. Rev. B 35 (14) (1987) 7423–7442.
[18] X. Zhou, R. Johnson, H. Wadley, Misfit-energy-increasing dislocations in vapor-deposited CoFe/NiFe multilayers, Phys. Rev. B 69 (14) (2004), 144113–0.
[19] H. Loulijat, H. Zerradi, S. Mizani, E. Achhal, et al., The behavior of the thermal conductivity near the melting temperature of copper nanoparticle, J. Mol. Liq. 211 (2015) 695–704.
[20] C. Oostenbrink, A. Villa, A.E. Mark, et al., A biomolecular force field based on the free enthalpy of hydration and solvation: the GROMOS force-field parameter sets 53A5 and 53A6, J. Combin. Chem. 25 (2004) 1656–1676.
[21] Q. Rong, C. Shao, H. Bao, Molecular dynamics study of the interfacial thermal conductance of multi-walled carbon nanotubes and Van Der Waals force induced deformation, J. Appl. Phys. 121 (2017), 054302.
[22] H. Heinz, R.A. Vaia, B.L. Farmer, et al., Accurate simulation of surfaces and interfaces of face-centered cubic metals using 12− 6 and 9− 6 Lennard-Jones potentials, J. Phys. Chem. C 112 (44) (2008) 17281–17290.
[23] V.P. Filippova, S.A. Kunavin, M.S. Pugachev, Calculation of the parameters of the Lennard-Jones potential for pairs of identical atoms based on the properties of solid substances, Inorganic Materials Applied Research 6 (1) (2015) 1–4.
[24] F.T. Smith, Atomic distortion and the combining rule for repulsive potentials, Phys. Rev. 5 (1972) 1708–1713.
[25] S. Plimpton, Fast parallel algorithms for short-range molecular dynamics, J. Chem. Phys. 117 (1995) 1–19.
[26] N.S. Mountain, Velocity Verlet algorithm for dissipative-particle-dynamics-based models of suspensions, Phys. Rev. 59 (3) (1999) 3733.
[27] W.M. Brown, A. Kohlmeyer, S.J. Plimpton, et al., Implementing molecular dynamics on hybrid high performance computers–particle–particle particle-mesh, Comput. Phys. Commun. 183 (3) (2012) 449–459.
[28] P. Wirnsberger, D. Frenkel, C. Dellago, An enhanced version of the heat exchange algorithm with excellent energy conservation properties, J. Chem. Phys. 143 (2015), 124104.
[29] T. Ikeshoji, B. Hafskjold, Non-equilibrium molecular dynamics calculation of heat conduction in liquid and through liquid-gas interface, Mol. Phys. 81 (1994) 251–261.
[30] B. Feng, L.W. Fan, Y. Zeng, Contribution of the hydroxyl group on interfacial heat conduction of monohydric alcohols: a molecular dynamics study, ASME Journal of Heat Transfer 142 (3) (2020), 031401.
[31] K. Sääskilahti, J. Oksanen, S. Volz, et al., Frequency-dependent phonon mean free path in carbon nanotubes from nonequilibrium molecular dynamics, Phys. Rev. B 91 (2015), 115426.
[32] S.H. Li, X.X. Yu, H. Bao, et al., High thermal conductivity of bulk epoxy resin by bottom-up parallel-linking and strain: a molecular dynamics study, J. Phys. Chem. C 122 (24) (2018) 13140–13147.
[33] J.J. Shi, Y.L. Dong, T. Fisher, et al., Thermal transport across carbon nanotube-graphene covalent and van der Waals junctions, J. Appl. Phys. 118 (4) (2015) 44302, 44302.
[34] T. Ohara, Contribution of intermolecular energy transfer to heat conduction in a simple liquid, J. Chem. Phys. 111 (1999) 9667–9672.
[35] A. Vasu, F.Y. Hagos, R. Mamat, et al., The effect of thermal cyclic variation on the thermophysical property degradation of paraffin as a phase changing energy storage material, Appl. Therm. Eng. 149 (2019) 22–33.
[36] Y. Chen, C. Zhang, Role of surface roughness on thermal conductance at liquid–solid interfaces, Int. J. Heat Mass Tran. 78 (2014) 624–629.
[37] T.Y. Lin, S.G. Kandlikar, An experimental investigation of structured roughness effect on heat transfer during single-phase liquid flow at microscale, ASME Journal of Heat Transfer 134 (10) (2012), 101701.
[38] S. Gang, J. Zhang, Y. He, et al., Thermal conductivity of carbon nanoring linked graphene sheets: a molecular dynamics investigation, Chin. Phys. B 26 (2017) 378–383, 010.